From T Associations to Pre-Biosignatures: How Ambartsumian's Paradigm of an Active, Evolving Universe Shapes the Search for Life in the Solar Neighborhood

V.S. Airapetian*[1,2]

[1]NASA Goddard Space Flight Center, Sellers Exoplanet Environments Collaboration, Greenbelt, MD 20771, USA
[2]Department of Physics, American University, Washington, DC 20016, USA

Abstract

Eighty years ago, Victor Ambartsumian founded the Byurakan Astrophysical Observatory and, within a year, overturned the prevailing view of a static stellar Universe by showing that stars are born in loose, expanding groups, the stellar associations, and that star formation is an ongoing process. The young T Tauri and flare stars that Byurakan studied for decades are now recognized as the magnetically active progenitors of the host stars of exoplanets. In this invited review, I trace how this paradigm evolved into a physically grounded program to search for life in the Universe. Over the last decade, my collaborators and I have built a chain of observations, models, and laboratory experiments linking young, rapidly rotating Sun-like stars to the chemistry of the atmospheres of their planets. Kepler, TESS, HST, Chandra, NICER and ground-based spectroscopy show that young solar analogues produce frequent superflares, intense X-ray and extreme-ultraviolet (XUV) emission, and coronal mass ejections (CMEs). Data-driven magnetohydrodynamic models and shock-acceleration models translate these eruptions into fluxes of stellar energetic particles (StEPs) at planetary orbits. Atmospheric chemistry and climate models, together with proton-irradiation experiments, suggest that StEPs penetrate deep into N_2–CO_2–CH_4–H_2O atmospheres and produce nitrous oxide (N_2O), hydrogen cyanide (HCN), formaldehyde, formamide and amino acids, including glycine, far more efficiently than lightning, GCRs or ultraviolet light. Particle-produced N_2O can reach $\sim 10^3$ ppmv in the laboratory, with an extrapolated production of $\sim 2\times10^{10}$ kg yr^{-1} on early Earth and may help resolve the faint young Sun paradox. I argue that the products of this space-weather-driven chemistry constitute *pre-biosignatures*: observable tracers of the conditions that precede life. I outline how JWST, the Extremely Large Telescope, a ground–space starshade hybrid and the Habitable Worlds Observatory could detect them.

Keywords: *stars: pre-main sequence – stars: flares – stars: coronal mass ejections – planets and satellites: atmospheres – astrobiology – history of astronomy*

1. Introduction: the grand question

"Are we alone in the Universe?" is one of the oldest questions humans have asked, and only recently has it become a question that can be observationally tested. Answering it requires two kinds of knowledge that were long developed separately. We must know where planets form and how their host stars behave. We must also understand what physical and chemical conditions allow a planetary surface to move from simple inorganic chemistry to prebiotic chemistry and biology. The first is a question about stellar evolution, which Byurakan helped to transform. The second is a question for planetary science, chemistry, and biology. Over the last ten years, the interdisciplinary community has argued that the two questions are tightly linked. The magnetic activity of a young star controls not only whether its planets may keep their atmospheres but also whether those atmospheres may develop the chemistry that leads towards life.

This paper accompanies my invited talk at the conference marking the 80th anniversary of the Byurakan Astrophysical Observatory (BAO), held in September 2026. Its goal is to show how the paradigm change introduced by Victor Ambartsumian in the 1940s, that stars are young, dynamic, and still forming around us, grew into today's search for life on exoplanets. Section 2 recalls the first revolution, the discovery of stellar

*vladimir.airapetian@nasa.gov

associations. Section 3 describes the second revolution brought by Kepler and other space observatories: exoplanets and superflares on Sun-like stars. Section 4 discusses the magnetic origin of stellar activity. Section 5 describes the eruptive space weather of young suns. Sections 6 and 7 show how energetic particles from this activity drive atmospheric escape and prebiotic chemistry, as tested in the laboratory. Section 8 introduces pre-biosignatures and the observatories that could detect them. Section 9 provides a summary of the main points of this paper.

2. Revolution I: Byurakan Observatory and the discovery of a young, active Galaxy

In 1945 Alfred Joy, working with the 100-inch telescope at Mount Wilson, identified a new class of irregular variable stars, the T Tauri stars. They revealed strong, variable Balmer and Ca II H and K emission lines and were associated with dark clouds (Joy, 1945). This was a new spectroscopic class, but its evolutionary meaning was unclear. The key step came from Byurakan. In 1947, a year after he founded BAO, Ambartsumian showed from a dynamical argument, not a new observation, that the O–B stars and the T Tauri stars form loose groups, which he called O associations and T associations. These groups are gravitationally unbound. Galactic tidal forces must disrupt them on time scales of order 10^7 years, so their members must be young. Star formation, therefore, did not happen only in the distant past. It is happening now, in groups, in our Galactic neighborhood (Ambartsumian, 1947, 1949).

This was a conceptual revolution. It replaced the picture of a static stellar population with one of continuous, dynamic evolution. It also marked T Tauri stars as signposts of extreme youth and, as later work showed, of intense magnetic activity. BAO's own instruments then turned this idea into an observational program (Figure 1). The 1-m Schmidt telescope, in operation from 1960, carried out wide-field Hα and photographic surveys that found new members of T associations and many flare stars. The 2.6-m telescope, in operation from 1975, provided spectroscopic follow-up of flare stars and T Tauri stars. The 1-m Schmidt, now modernized with a CCD detector, is still used for surveys of young stars and Herbig–Haro objects. Byurakan's long-term studies of flare stars in associations and young clusters established, decades before the term existed, that young stars are dominated by magnetically driven eruptions. As shown below, this is exactly the property that now governs the environments of young planets.

There is also a striking astrophysical link between Ambartsumian's associations and our own Solar System. Three-dimensional maps of nearby star-forming regions show that almost all young stars within ∼200 pc lie on the surface of the Local Bubble, a cavity carved by supernovae, whose expansion swept up gas and triggered the formation of the T-association-like groups around us over the last ∼14 Myr (Zucker et al., 2022). The Sun therefore currently resides inside a structure shaped by the same kind of young stellar groups that Ambartsumian identified. The passage of the Sun through such environments changes the flux of Galactic cosmic rays and the energetic particle environment of the Earth, which is relevant to the particle driven chemistry discussed in Section 6.

3. Revolution II: exoplanets and superflares

3.1. Kepler and superflares on Sun-like stars

The second revolution came with space optical photometry. The Kepler mission (Borucki et al., 2010) found more than 2,600 confirmed exoplanets by the transit method and discovered that rocky planets in the habitable zones of Sun-like (F-G-K) and M dwarf stars are common. The same high-precision light curves also revealed something unexpected. Maehara et al. (2012) found 365 superflares, with energies of 10^{33}–10^{36} erg, on 148 solar-type stars. These events are 10–10^3 times more energetic than the largest solar flares recorded. Most of them occurred on rapidly rotating, and therefore young, stars, which typically show large starspots. Kepler light curves of young solar-type stars (Figure 2a) show rotational modulation by large spots, with frequent superflares on top of it. For old, slowly rotating Sun-like stars, superflares with energies above $\sim 10^{34}$ erg is estimated to occur once per century to once per several millennia (Okamoto et al., 2021, Vasilyev et al., 2024). For young solar-like stars, they are far more frequent and energetic.

Byurakan's young, magnetically active stars are therefore today's exoplanet host stars. Three decades after the discovery of 51 Peg b, the NASA Exoplanet Archive (Akeson et al., 2013) lists more than 6,400 confirmed exoplanets (as of October 2026), most of them found by the transit method with Kepler, K2

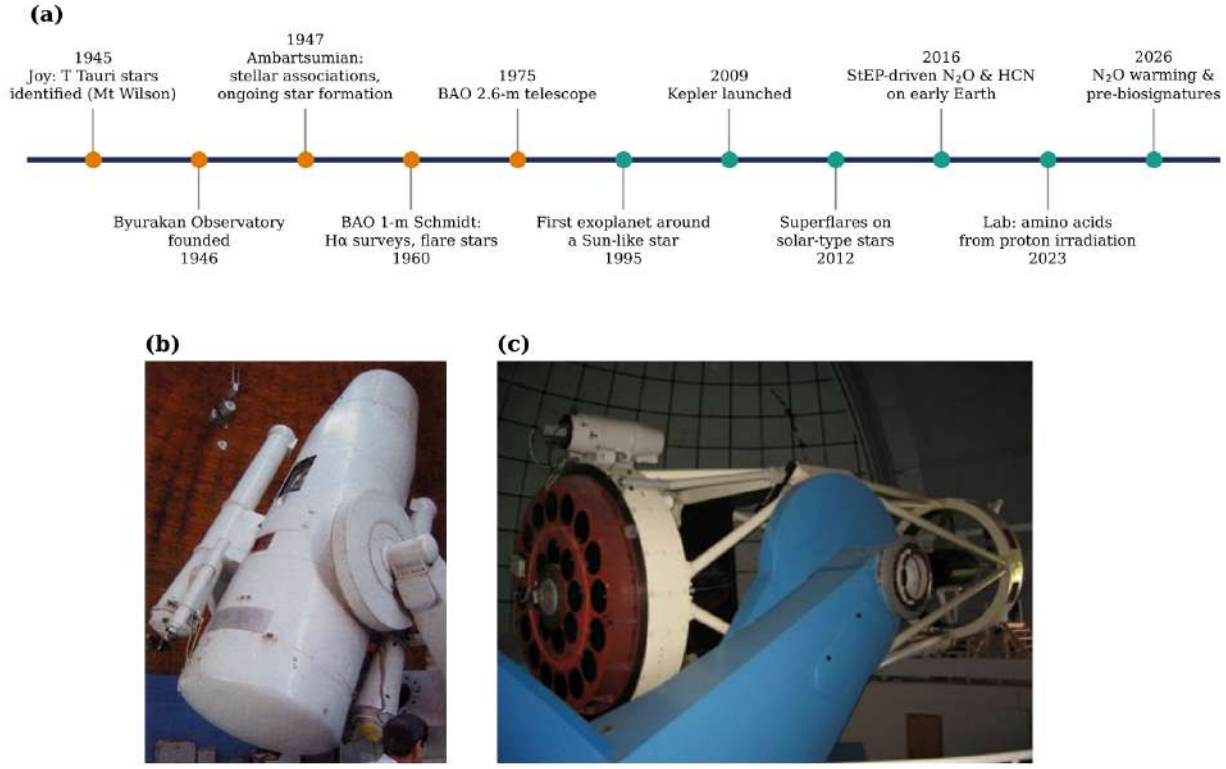

Figure 1. Byurakan's legacy in context. (a) Milestones from Joy's identification of T Tauri stars and Ambartsumian's discovery of stellar associations to recent results on space-weather-driven prebiotic chemistry. (b) The BAO 1-m Schmidt telescope (1960), used for wide-field Hα surveys of T associations and flare stars. (c) The BAO 2.6-m telescope (1975), used for spectroscopic follow-up of flare stars and T Tauri members.

and TESS. When the count passed 6,000 in September 2025, about 700 of these planets were classified as terrestrial, that is, rocky planets of roughly Earth size or smaller, and about 1,760 as super-Earths. Occurrence rates corrected for detection biases show that small planets are the rule rather than the exception, and that they become more common toward cooler stars. About 30% of Sun-like stars host Kepler-like systems of planets larger than Earth with periods shorter than 400 d, with ∼3 planets per system (Zhu and Dong, 2021, Zhu et al., 2018). The fraction of stars that host inner planetary systems of 0.5–10 $R_\oplus$ rises from ∼32% for F2 dwarfs to ∼57% for G2 dwarfs and ∼96% for mid-K dwarfs (He et al., 2021). Planets of 1–4 $R_\oplus$ are about twice as common around M dwarfs as around G dwarfs and three times as common as around F dwarfs (Howard et al., 2012, Mulders et al., 2015), and an M dwarf hosts on average 2.5 ± 0.2 such planets with periods shorter than 200 d (Dressing and Charbonneau, 2015). For terrestrial planets in the habitable zone (HZ), Kepler data give $\eta_\oplus \approx 0.37$–0.60 rocky (0.5–1.5 $R_\oplus$) planets per Sun-like G or early-K dwarf in the conservative HZ, which implies ∼4 such planets around G and K dwarfs within 10 pc of the Sun (Bryson et al. 2021; see also Petigura et al. 2013). For M dwarfs the conservative HZ holds ≈0.16 Earth-size planets per star, rising to ≈0.24 for the optimistic HZ boundaries (Dressing and Charbonneau, 2015). Because M dwarfs make up ∼70% of the stars within 10 pc of the Sun (Henry et al., 2006), most nearby terrestrial HZ planets are expected to orbit M dwarfs, which remain magnetically active for billions of years. All of these planets once orbited young, rapidly rotating and flaring stars, and a growing number are now observed while their hosts are still young, including AU Mic b (∼22 Myr; Plavchan et al. 2020), the four planets of V1298 Tau (∼23 Myr; David et al. 2019) and DS Tuc Ab (∼45 Myr; Section 3.4).

To quantify what a young planet experiences, our group has combined photometric, spectroscopic and X-ray monitoring with modelling. The best-studied young solar analogue, EK Draconis (age ∼50–120 Myr), rotates with a period of 2.77 d. Ikuta et al. (2026) compared starspot maps derived from TESS photometry with Zeeman–Doppler magnetic maps. They found that the spot locations largely agree, except for a polar spot, and that the Hα variability follows the spots while the X-ray variability does not, because it is dominated by multiple active regions and extended coronal structures.

3.2. XUV evolution of the young Sun

The X-ray and extreme-ultraviolet (XUV) radiation of a young star heats and expands planetary upper atmospheres and drives escape. Since EUV radiation longward of ∼36 nm is absorbed by the interstellar medium, it must be reconstructed. Using HST observations of 23 solar-type stars and an N V-based scaling, France et al. (2025) derived the EUV history of the Sun from 10 Myr to 10 Gyr (Figure 2b). The fractional EUV luminosity is saturated at $L_{\rm EUV}/L_{\rm bol} \approx 10^{-4}$ up to a break at ∼73 Myr and then declines as a power law with index -1.12 ± 0.06. The EUV flux at 1 au was ∼100 times the present value at 10 Myr. Early M dwarfs stay saturated 10–20 times longer and at a higher level, which is critical for the habitability of their planets.

3.3. Megaflares from pre-main-sequence stars and their disks

Chandra studies of young clusters extend this picture to the pre-main-sequence (PMS) phase studied in Byurakan's associations. Getman and Feigelson (2021) analyzed more than a thousand X-ray superflares and megaflares from stars younger than ∼5 Myr in 40 star-forming regions, with energies up to $\sim 10^{38}$ erg. PMS flares are 3 to 6 orders of magnitude more powerful than the solar Carrington event and occur roughly a million times more often than large flares on the present Sun. A natural question is whether such flares require abnormally strong magnetic fields. In the Multi-Observatory Research of Young Stellar Energetic Flares (MORYSEF) campaign, which combined Chandra, HET-HPF, VLBA and ALMA observations of Orion stars (Getman et al., 2024), Getman et al. (2025) measured average surface fields of ∼2.4–3 kG after powerful flares, which is typical for non-flaring PMS stars. The large X-ray luminosities of PMS flares instead follow from much larger active regions and flaring loop volumes. How these flares compare with the relation between X-ray luminosity and unsigned magnetic flux followed by the Sun and other stars (Figure 2c) is discussed in Section 4.

Megaflares also affect the protoplanetary disks in which planets form. ALMA has revealed rings and gaps in many disks around T Tauri stars, where accretion is controlled by stellar magnetic fields. Multi-epoch ALMA observations of the disk around the T Tauri star IM Lup gave the first evidence that stellar flares can change disk chemistry on short time scales (Cleeves et al., 2017). The disk-integrated $H^{13}CO^+$ $J = 3$–2 intensity doubled in one epoch, while the dust continuum remained constant. Time-dependent chemical models showed that a large or prolonged stellar X-ray flare can temporarily raise the ionization of the upper disk atmosphere and enhance the HCO^+ abundance there. Stellar energetic particles (StEPs) that accompany large flares provide a further, and in the disk surface possibly dominant, source of ionization. Rab et al. (2017) used the thermo-chemical disk code ProDiMo (Woitke et al., 2009) to model a T Tauri disk irradiated by a proton spectrum derived from solar particle events and scaled up by a factor of $\sim 10^5$, as suggested by the X-ray flare activity of young stars (Feigelson et al., 2002). This corresponds to $\sim 1.5 \times 10^7$ protons cm^{-2} s^{-1} above 10 MeV at 1 au. The particles do not reach the disk midplane, but they dominate the H_2 ionization of the upper disk layers, including the warm molecular layer, with ionization rates of $\gtrsim 10^{-12}$ s^{-1} close to the star. They raise the column densities of HCO^+ and N_2H^+ by factors of ∼3–10 within ∼200 au, with the largest effect when the ionization by Galactic cosmic rays is low. Rab et al. (2017) also pointed out that individual powerful particle and X-ray flares should leave transient signatures in molecular ions that only multi-epoch observations can reveal, a prediction consistent with the variability detected in IM Lup. Spatially resolved observations of molecular ions that trace different disk layers can therefore separate the contributions of StEPs, X-rays and cosmic rays, and constrain the particle flux of young stars. Disk chemistry, and therefore the composition of the planets that form in the disk, carries an imprint of stellar magnetic activity.

3.4. Far-ultraviolet flares on DS Tuc A

Far-ultraviolet (FUV) flares are especially important for atmospheric photochemistry. New HST observations of the ∼45 Myr old most active young active G6V member of the ∼40-Myr Tucana-Horologium DS Tuc A, which hosts a transiting planet, show a remarkably high FUV flare rate (Sextro et al., 2026). In only 7.2 ks of observation, 25 flares were detected in the Si IV lines and 21 in N V, but none in the hot coronal Fe XXI line (Figure 3). This corresponds to more than 50 large FUV flares per day, comparable in FUV energy to solar X-class flares. Thus, a planet around such a star, DS Tuc Ab, a ∼5.6–5.7 $R_\oplus$ mini-Neptune is exposed to quasi-continuous flaring. This combination, a mini-Neptune-class warm inflated atmosphere around one of the youngest, most active young solar analog planet hosts accessible to JWST makes

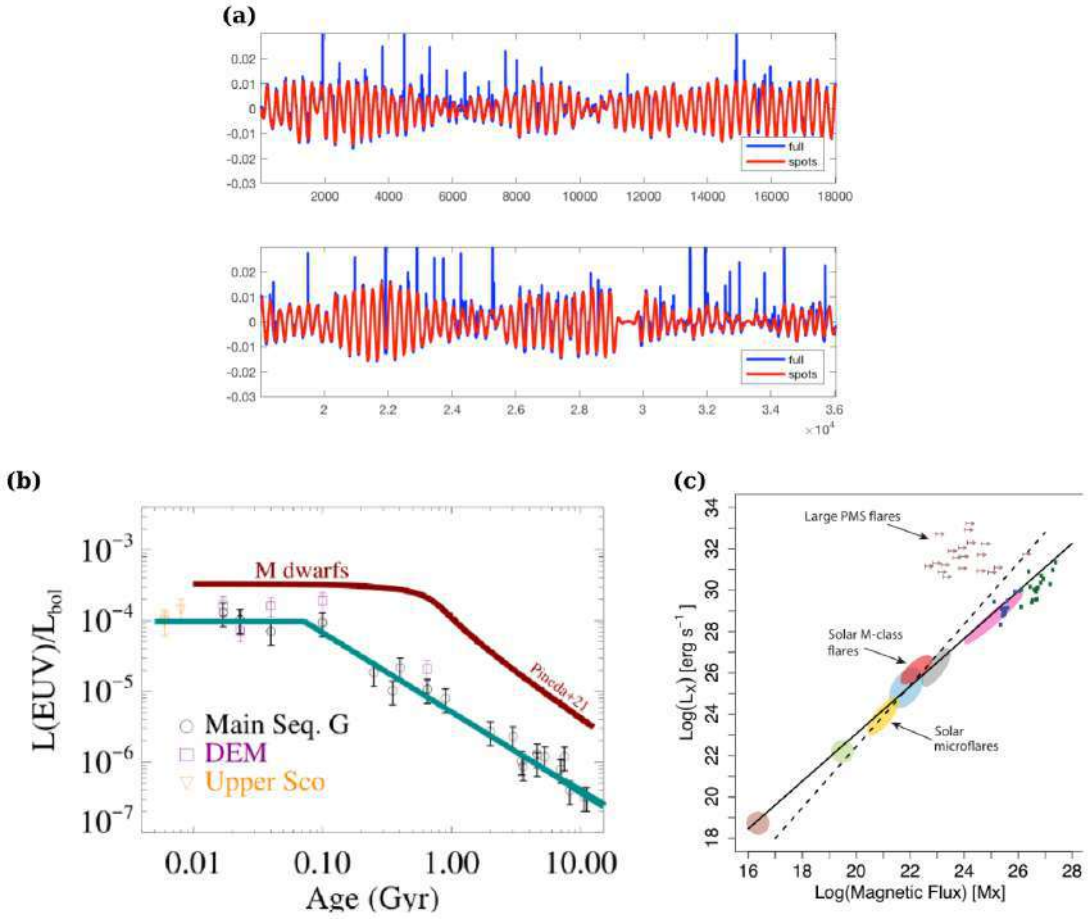

Figure 2. Young solar-type stars as exoplanet hosts. (a) Kepler light curve of a young solar-type star: rotational modulation by starspots (red, spot model) with frequent superflares (blue spikes; full light curve). (b) Fractional EUV (90–360 Å) luminosity of solar analogues as a function of age, with the comparable M-dwarf evolution (from France et al. 2025). (c) X-ray luminosity versus unsigned magnetic flux from solar microflares to large PMS flares (from Getman et al. 2025).

DS Tuc Ab a unique laboratory for testing whether extreme stellar XUV radiation and energetic-particle forcing measurably shape the photochemistry and aerosol properties of young exoplanet atmospheres.

4. The magnetic origin of stellar activity: universal scaling laws

To use the Sun as a calibrator for other stars, we need laws that connect magnetic flux to radiative output. Using ten years of Sun-as-a-star data, Toriumi and Airapetian (2022) showed that the irradiance in a wide range of X-ray, EUV, FUV and chromospheric lines scales as a power law of the total unsigned magnetic flux. The indices are ∼1.1–1.4 for coronal emission and ∼0.8–0.9 for chromospheric emission. The same relations hold for G-type stars with ages of 50 Myr to 4.5 Gyr. Toriumi et al. (2022) extended this to further activity proxies and more spectral lines, and Namekata et al. (2023) used the relations to reconstruct the full 0.1–180 nm XUV and FUV spectra of EK Dra, π^1 UMa and κ^1 Ceti from their magnetic fluxes. The reconstructions agree with observations to within an order of magnitude. These scaling laws provide the high-energy spectral input for the atmospheric models described below, including in the unobservable EUV band. They also show that solar and stellar flares are magnetically controlled phenomena of the same physical nature.

Pre-main-sequence stars extend these relations to the most extreme magnetic activity. Across solar magnetic elements, the Sun as a star, older active stars and PMS stars, the X-ray luminosity follows a single baseline power law, $L_X \propto \Phi^m$ with $m \approx 1.15$ (Pevtsov et al., 2003), and the time-averaged L_X and Φ of PMS stars lie 4–5 orders of magnitude above those of the present Sun, reflecting the greater efficiency of their fully convective dynamos (Getman et al., 2025). The most powerful PMS super- and megaflares, however, lie well above this baseline. Flare models based on X-ray data alone placed their L_X 10^3–10^4 times above the

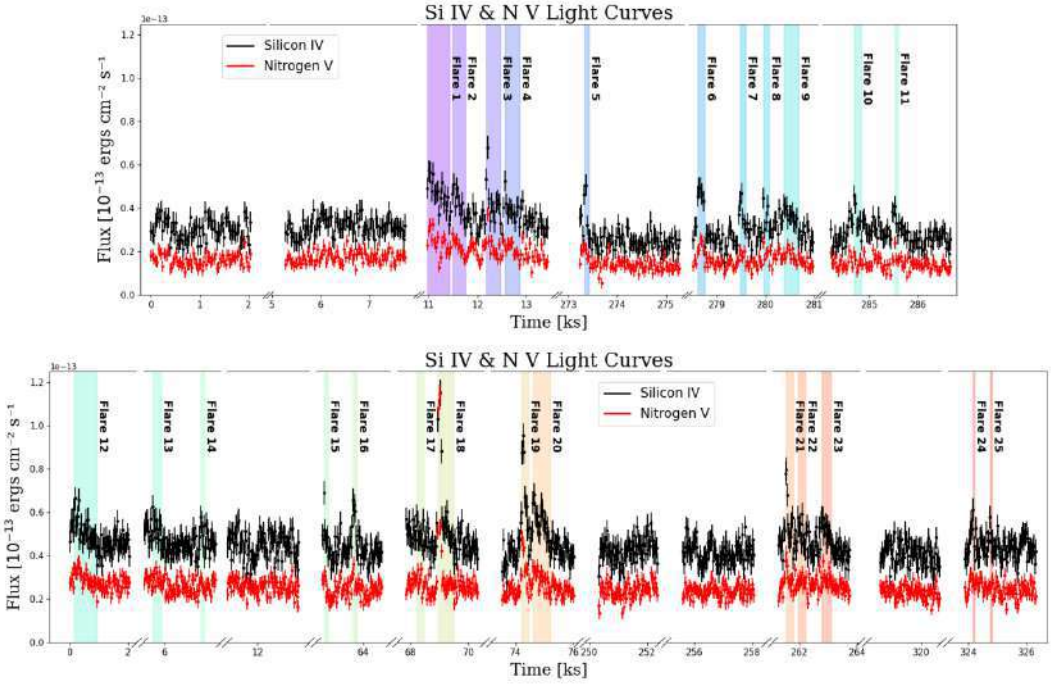

Figure 3. HST light curves of DS Tuc A in the Si IV (black) and N V (red) transition-region lines. Shaded intervals mark detected flares (25 in Si IV and 21 in N V in 7.2 ks of exposure; Sextro et al. 2026).

scaling-law prediction, and 3D MHD models of active-region coronae, which give $L_X \propto \Phi^{3.4}$ when only the field strength is varied (Zhuleku et al., 2021), could explain this only with active-region fields of ∼10–20 kG. Getman et al. (2025) tested this hypothesis directly in the MORYSEF campaign, with nearly simultaneous Chandra X-ray and HET-HPF Zeeman-broadening observations of four M-type PMS stars in the Orion Nebula caught during or just after super- and megaflares. Their average surface fields (Section 3.3) are typical of non-flaring PMS stars, which rules out abnormally strong fields. Combining the measured fields with Monte Carlo models of the flaring loops, they placed the flares on the L_X–Φ diagram (Figure 2c). The flare fluxes span $\sim 10^{22}$–10^{26} Mx, and the peak L_X values lie 1 to 4–5 orders of magnitude above the baseline law. Solar M- and X-class flares deviate in the same sense but less, by ∼1.5 orders of magnitude, and solar microflares alone already follow a steeper relation, $L_X \propto \Phi^3$ (Kirichenko and Bogachev, 2017), so that flares as a class have $1.5 \lesssim m \lesssim 4$. Compared with large solar flares, PMS flares have ∼2–4 dex larger magnetic fluxes and ∼4–6 dex higher peak X-ray luminosities. Because the field strengths are similar, these offsets arise from size. The footpoint areas of the PMS flaring loops are ∼3 dex larger, which accounts for the flux difference, and their emitting volumes are much larger, which accounts for a ∼4.5 dex difference in peak L_X. The ratios of free to potential magnetic energy in the PMS flaring loops are comparable to those of solar M- and X-class flares, and the loops are preferentially dipolar and extend to several stellar radii, consistent with Zeeman–Doppler maps and MHD models of fully convective stars. Large PMS flares are therefore scaled-up analogues of solar flares. Getman et al. (2025) suggest that the deviation of flares from the baseline relation arises because flares are powered by magnetic reconnection, which converts magnetic flux into X-rays more efficiently than the mechanisms that may sustain the quiescent corona, such as Alfvén-wave heating. For young planets this means that the magnetic flux of the host star sets both its quiescent XUV output and, through the size of its active regions, the energy of its largest flares.

5. Space weather of young suns: CMEs and energetic particles

5.1. Searching for stellar coronal mass ejections

On the Sun, the largest flares are usually accompanied by CMEs, which drive shocks that accelerate solar energetic particles (SEPs). Whether CMEs also accompany superflares on young suns is crucial for planets, because CMEs and particles, not photons, dominate atmospheric erosion and ionization at depth. In a 12-day TESS–NICER–Seimei campaign on EK Dra, Namekata et al. (2024) detected three superflares with energies of 1.5×10^{33}–1.2×10^{34} erg. They also detected blueshifted Hα emission from two prominence

eruptions, with velocities of ∼690 and ∼430 km s^{-1} and masses of ∼1.1×10^{19} g and ∼3.2×10^{17} g (Figure 4). The faster eruption was followed by a possible X-ray dimming of up to ∼10%, a signature of a fast CME that evacuates coronal plasma. More recently, combined HST FUV and ground-based Hα spectroscopy of a Carrington-class (∼10^{32} erg) flare on EK Dra revealed a multi-temperature CME. Warm (∼10^5 K) plasma moved at 300–550 km s^{-1}, followed about ten minutes later by a cool (∼10^4 K) filament eruption at ∼70 km s^{-1} (Namekata et al., 2025).

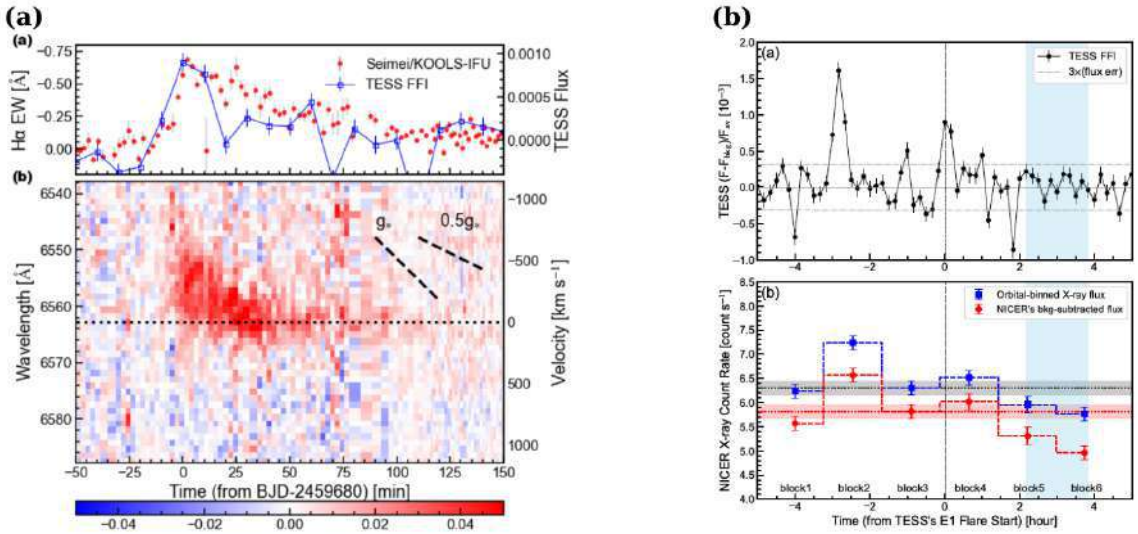

Figure 4. Prominence eruption and X-ray dimming on the young solar analogue EK Dra (Namekata et al., 2024). (a) Hα equivalent width and TESS flux, and the dynamic Hα spectrum showing blueshifted emission from an erupting prominence. (b) TESS light curve and NICER X-ray count rate around the flare. The decrease after the flare (shaded) is consistent with coronal dimming caused by a CME.

5.2. Data-driven models of young coronae and CMEs

To translate such observations into planetary space weather, we developed three-dimensional magneto-hydrodynamic (MHD) models of the coronae and winds of young suns, driven by observed Zeeman–Doppler magnetic maps. For the ∼600 Myr old solar twin κ^1 Ceti, maps from two epochs 11 months apart give a hot, dense corona and a fast wind. The resulting co-rotating interaction regions exert dynamic pressures ∼1300 times higher than those observed at the present Sun (Airapetian et al., 2021). Such pressures would strongly compress the magnetospheres of early Venus, Earth and Mars. In ongoing work, we insert a bipolar active region into the observed magnetic map and energize a twisted, unstable magnetic flux rope with ∼2×10^{34} erg of free energy. The flux rope erupts as a fast CME, which drives a shock with speeds of several thousand km s^{-1} through the young stellar wind (Figure 5).

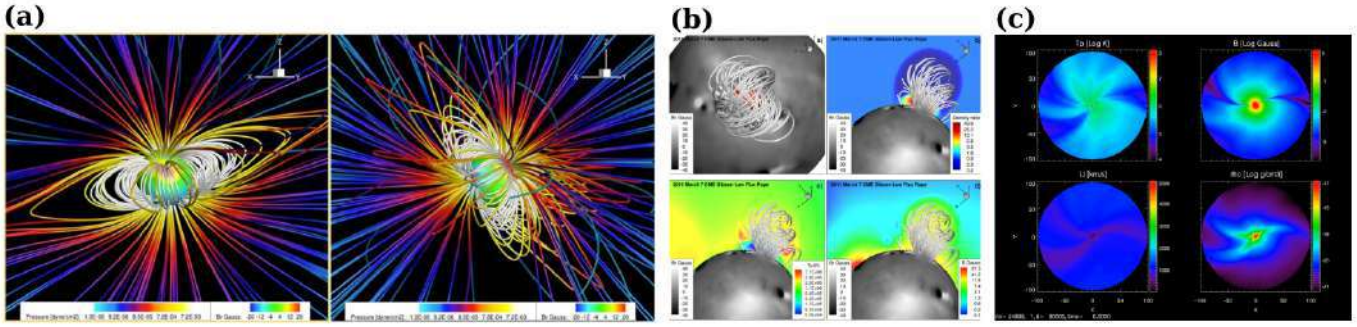

Figure 5. Three-dimensional MHD modelling of a young Sun's corona and CMEs. (a) Magnetic skeleton of the corona of a young solar analogue driven by an observed magnetic map, before and after inserting an active region (Airapetian et al. 2021, and work in progress). (b) A twisted, unstable flux rope (Gibson–Low type) used to launch a CME. (c) Temperature, magnetic field, velocity and density in the equatorial plane after the eruption of the flux rope.

doi: https://doi.org/10.52526/25792776-26.73.2-375

5.3. CME shocks as the source of stellar energetic particles

On the Sun, the largest gradual SEP events are produced by diffusive shock acceleration at CME-driven shocks. Hu et al. (2022) used the improved Particle Acceleration and Transport in the Heliosphere (iPATH) model to simulate twelve superflare-associated CMEs with energies of 10^{32}–10^{35} erg and speeds of 1500–7500 km s^{-1}. They found that the peak >10 MeV proton flux scales with the peak soft X-ray flux of the flare as $F_{\rm p} \propto F_{\rm SXR}^{0.77}$, and that the event-integrated spectra of the fastest CMEs extend to GeV energies (Figure 6b). Such StEP events are not purely theoretical even for the modern Sun. Cosmogenic isotopes record extreme solar particle events in 994 CE, 775 CE, 660 BCE and 7176 BCE (Koldobskiy et al., 2023, Miyake et al., 2012). Their integral fluences exceed those of the strongest instrumentally recorded ground-level enhancements by one to two orders of magnitude (Figure 6a). For the young Sun, events at least this strong would have been routine.

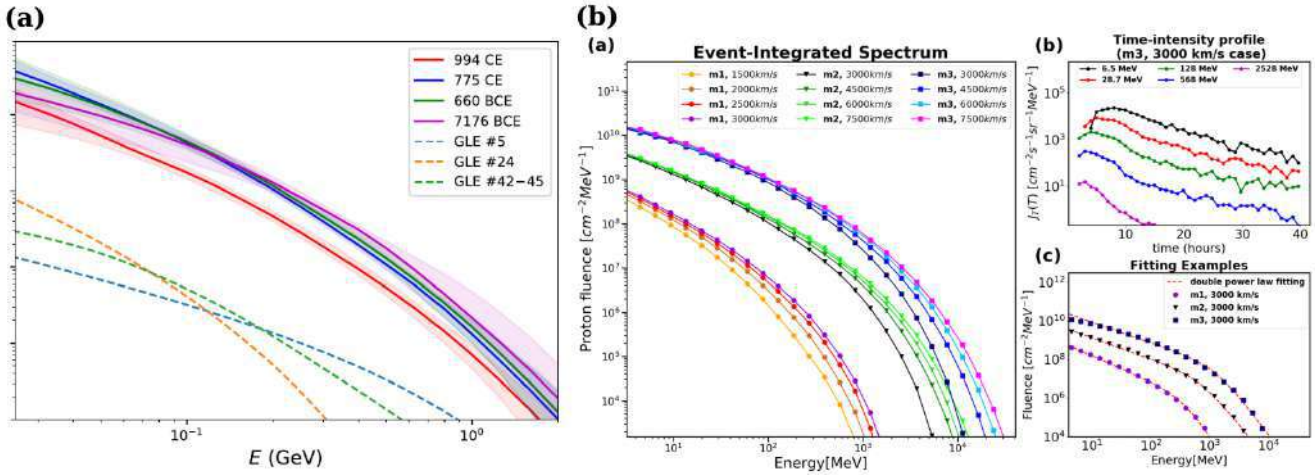

Figure 6. Energetic-particle spectra of solar and stellar superflares. (a) Integral spectral fluences of extreme solar particle events reconstructed from cosmogenic isotopes (solid) compared with ground-level enhancements recorded by instruments (dashed) (Koldobskiy et al., 2023). (b) Event-integrated proton fluence spectra at 1 au from iPATH simulations of superflare-driven CMEs with speeds of 1500–7500 km s^{-1} (Hu et al., 2022).

6. A double-edged sword: atmospheric escape and catalysis

The same stellar activity acts on young planetary atmospheres in two opposite ways. On one side is erosion. XUV heating expands and inflates upper atmospheres, and thermal and non-thermal processes remove atmospheric species. Ionized outflows along open magnetic field lines, polar rain and magnetosheath precipitation all add to atmospheric loss, and repeated superflares and CMEs can strip primordial H/He envelopes. For planets in the habitable zones of active stars, ion escape driven by stellar XUV radiation and CMEs can remove a large part of an Earth-like atmosphere on geologically short time scales (Airapetian et al., 2017, 2020, Gronoff et al., 2020).

Erosion is driven not only by discrete eruptions but also by persistent structures in the stellar wind. In the winds of young, rapidly rotating suns, fast coronal-hole streams overtake slower, denser wind and form corotating interaction regions (CIRs) bounded by strong shocks. Because CIRs corotate with the star, a planet crosses them every rotation. Sur and Airapetian (2025) used the Space Weather Modeling Framework (SWMF/Geospace), coupled with the Rice Convection Model, to follow the response of the early Earth's magnetosphere and ionosphere to the CIR shock in our data-driven wind model of κ^1 Ceti (Section 5.2; Airapetian et al. 2021). The CIR carries proton densities of up to ∼1800 cm^{-3}, about 18 times those of present-day extreme events, and dynamic pressures of up to ∼2100 nPa, so the pressure pulse is driven by density rather than speed. The dayside magnetopause moves in to ∼3 $R_{\rm E}$, about 40% closer to the planet than during the May 2024 superstorm. The SYM-H index reaches ∼ −700 nT, comparable to the March 1989 storm, the cross-polar-cap potential reaches ∼390–460 kV, and the polar cap expands to ∼41–43° colatitude. Hemispherically integrated Joule heating peaks at ∼4 TW, and the energy dissipated in each hemisphere during the ∼2-day passage, ∼(1.9–2.6)×10^{17} J, is comparable to or larger than the total NO

doi: https://doi.org/10.52526/25792776-26.73.2-375

and CO_2 infrared cooling of the thermosphere during the four days of the May 2024 storm. Precipitating electrons reach energies of ∼300–400 keV and can penetrate below ∼70 km. A storm of the May 2024 class occurs today about once per solar cycle, or ∼0.1% of the time, whereas the early Earth would have spent ∼11–14% of its time inside such CIRs.

For a younger Sun the forcing is stronger still. Sur et al. (2026) drove the same model with an Alfvén Wave Solar Model (AWSoM) wind of EK Dra (age 50–125 Myr, rotation period 2.7 d), whose CIR reaches a dynamic pressure of ∼6900 nPa and a southward field $B_z \approx -130$ nT. For the first time, they set the ionospheric conductance to a young-Sun EUV level, $F_{10.7} = 10^4$ sfu, a conservative 100-fold enhancement over present-day values. The magnetopause is compressed to 2.16 R_E, approaching the 1.5 R_E found for a CME from the young Sun (Airapetian et al., 2016). SYM-H reaches ~ -1600 nT, comparable to the Carrington storm. The polar cap expands to ≈51° colatitude, so that ∼60% of the planetary magnetic flux is open, and the auroral currents and electron precipitation move down to ∼40° magnetic latitude, a level reached today only in the most extreme historical storms. The cross-polar-cap potential peaks at 1.16 MV and the Joule heating at 28 TW, 5–7 times the κ^1 Ceti CIR and 3–4 times the May 2024 superstorm. A key result is that the EUV-enhanced conductance short-circuits the ionospheric dynamo. Compared with present-day illumination, it lowers the cross-polar-cap potential by 32–60% and the Joule heating by a factor of ≈2.2, so models of young planets that adopt present-day conductance overestimate the energy input.

Because EK Dra rotates in 2.7 d, a planet at 1 au lies inside CIR flows 37–48% of the time (Sur et al., 2026). Conditions that are once-a-century extremes today would then have been a routine, once-per-rotation state for the early Earth and for Earth-like exoplanets around young solar analogues. Joule heating at tens of TW raises ion scale heights, keV electron precipitation strengthens the ambipolar electric field that lifts heavy ions, and with ∼60% of the magnetic flux open these ions have direct escape channels. A magnetopause at ∼2 R_E also approaches the hydrodynamically expanded thermosphere expected under strong EUV irradiation, which could allow direct pick-up of exospheric ions by the stellar wind. CIRs are therefore as consequential as CMEs for the atmospheric loss of young habitable-zone planets (Sur and Airapetian, 2025, Sur et al., 2026). The same CIR shocks also accelerate ions, to ∼20 MeV nucleon^{-1} even in the present solar wind, and together with the compressed magnetosphere they give energetic particles access to the lower atmosphere at low latitudes. The unmagnetized young Moon would have been exposed to CIR particle fluxes ∼30–500 times of today's fluence, so ^{3}He, H_2O and OH implanted in buried lunar paleoregolith may preserve a record of this wind (Airapetian et al., 2026, Sur et al., 2026).

On the other side is chemical catalysis. Unlike XUV photons, which are absorbed in the thermosphere, StEPs with energies from tens of MeV to GeV penetrate into the lower atmosphere, sometimes down to the surface. There they produce cascades of secondary particles, including multiple generations of secondary electrons, ionizing and dissociating N_2, CO_2, CH_4 and H_2O (Figure 7). This releases a family of reactive radicals ($N(^4S)$, $N(^2D)$, OH, CH, NH) that recombine into molecules important for both climate and prebiotic chemistry. In a weakly reducing early Earth atmosphere, the main pathways are:

$$N_2 + e^-,\ p \rightarrow 2N(^4S) + e^-,\ p \tag{1}$$

$$N(^4S,\ ^2D) + O_2 \rightarrow NO + O(^3P) \tag{2}$$

$$H_2O + ion^+ \rightarrow H + OH + ion^+ \tag{3}$$

$$NO + NH \rightarrow N_2O + H \tag{4}$$

$$NO + CH \rightarrow HCN + O; \quad CH_2,\ CH_3 + N(^4S) \rightarrow HCN + H\ (+H) \tag{5}$$

$$HCN + H_2O \rightarrow H_2NCHO\ \text{(formamide)} \tag{6}$$

Airapetian et al. (2016) combined Kepler superflare statistics with SEP transport and a photochemical model of the early Earth atmosphere. They showed that frequent StEP events from the young Sun would have produced N_2O, a powerful greenhouse gas, and HCN, the key feedstock of prebiotic chemistry. Hydrolysis of HCN leads to formamide, and HCN-based cyanosulfidic chemistry can produce the precursors of nucleotides, amino acids and lipids (Patel et al., 2015). Flare-driven chemistry is also persistent. On planets around K and M dwarfs, repeated flares push the atmosphere into new chemical steady states, with NO_x, N_2O and HNO_3 as potentially observable products (Chen et al., 2021). The events that threaten an atmosphere may therefore also seed its prebiotic chemistry.

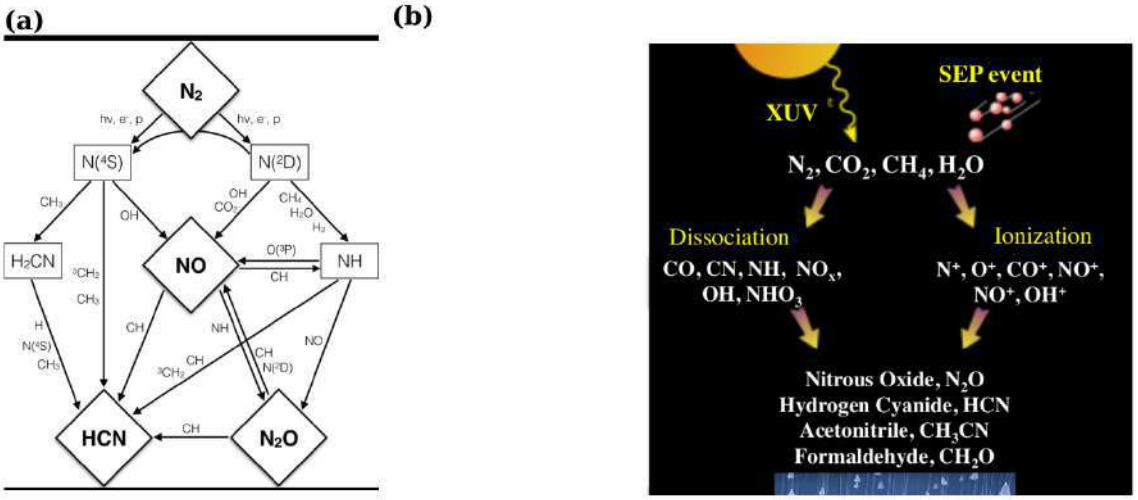

Figure 7. Space-weather-driven chemistry. (a) Simplified reaction network in which energetic particles (e^-, p) and photons dissociate N_2, producing NO, NH, N_2O and HCN. (b) Schematic of XUV and StEP-driven dissociation and ionization of N_2, CO_2, CH_4 and H_2O, leading to N_2O, HCN, acetonitrile and formaldehyde (after Airapetian et al. 2016).

7. Testing space-weather chemistry in the laboratory

Model predictions of particle-driven chemistry must be tested in the laboratory. With Kensei Kobayashi and colleagues at Yokohama National University, we irradiated mixtures of N_2, CO_2, CH_4 and liquid H_2O with MeV protons from a tandem accelerator, which simulate solar energetic particles. We compared the results with spark discharges, which simulate lightning, and with ultraviolet irradiation (Kobayashi et al., 2023). After acid hydrolysis, proton irradiation produced amino acids, including glycine, from mixtures with only 0.5% methane. Spark discharges needed at least 15% methane, and UV produced no detectable amino acids even at 50%. At a methane ratio of 0.2, the glycine G-value for protons was about 5,000 times higher than for spark discharges (Figure 8b). Carboxylic acids formed even in mixtures without methane. In the weakly reducing atmosphere now favored for the Hadean Earth, energetic particles from the young Sun would therefore have been a more effective energy source for prebiotic synthesis than lightning.

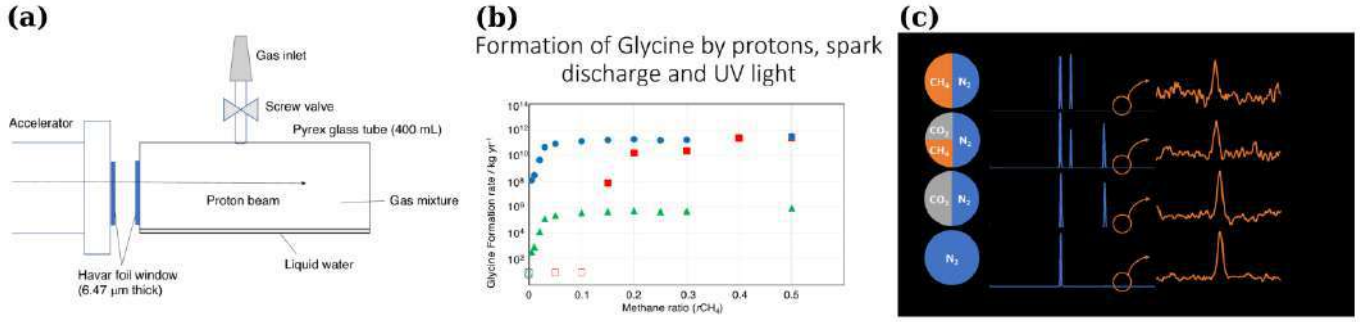

Figure 8. Laboratory simulation of StEP-driven chemistry. (a) Set-up for proton irradiation of a gas mixture above liquid water. (b) Glycine formation rates as a function of the methane mixing ratio. Proton irradiation (blue circles) produces glycine at much lower CH_4 fractions than spark discharges (red squares; open symbols are non-detections) (Kobayashi et al., 2023). (c) Gas chromatograms showing N_2O formed by proton irradiation in CH_4–N_2, CO_2–CH_4–N_2, CO_2–N_2 and pure N_2 mixtures (Kobayashi et al., 2026).

Kobayashi et al. (2026) extended these experiments to N_2O, using 1.5 MeV protons and $N_2/CO_2/CH_4/H_2O$ mixtures, including in the ExoPlanetary Particle Irradiation Chemistry (EPIC) set-up. N_2O formed in all mixtures, even in pure N_2 with water (Figure 8c), with mixing ratios of up to ~1000 ppmv. Extrapolated to the particle flux of the young Sun, this corresponds to a global N_2O production of $\sim 2\times10^{10}$ kg yr^{-1}. A photochemical model of StEP-driven irradiation reproduces the experimental production rates and gives self-consistent vertical profiles of N_2O, NO and NO_2 (Figure 9). These profiles were used as input to the ROCKE-3D general circulation model (Way et al., 2017). The faint young Sun paradox is that the Sun

doi: https://doi.org/10.52526/25792776-26.73.2-375

was ∼30% fainter 4 Gyr ago, yet geology shows liquid water (Feulner, 2012, Sagan and Mullen, 1972). Even an atmosphere with only 1% CO_2 and 100 ppmv N_2O gives a partially ice-free planet in which the warmest regions approach the melting point, a possible "cold start" for life. Frequent StEP events could therefore have helped resolve the paradox. They could also keep young rocky exoplanets temperate beyond the conventional outer edge of the habitable zone, while building up prebiotic molecules at the same time.

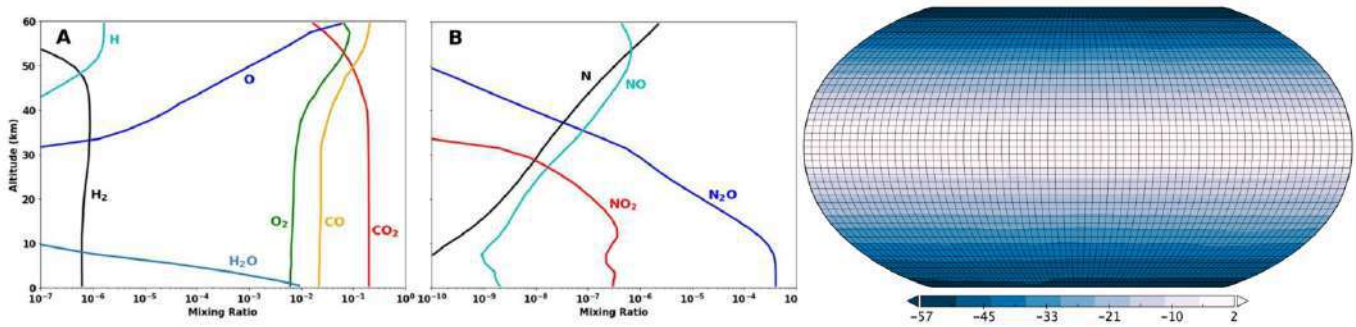

Figure 9. N_2O warming of a young rocky planet (Kobayashi et al., 2026). (A, B) Vertical mixing-ratio profiles of the main species and of StEP-produced N, NO, NO_2 and N_2O in a 1 bar N_2 atmosphere with 1% CO_2. Right: ROCKE-3D surface temperature map (°C) for 100 ppmv N_2O and no CH_4, with temperatures from about −60 °C to +2 °C.

8. Pre-biosignatures and how to observe them

The chain from Byurakan's young stars to prebiotic chemistry leads to a new observational target. Classical biosignatures, such as O_2, O_3 and CH_4 in disequilibrium, are expected only after life has become widespread. Habitable but still uninhabited planets may, however, be more common, and their atmospheres can be tested for the processes that precede life. I call the products of space-weather-driven chemistry *pre-biosignatures*: N_2O, HCN, NO_x, H_2CO, CH_3CN and related species whose abundances reflect the energetic particle environment, the nitrogen chemistry and the availability of prebiotic feedstock. Measuring them together with the stellar XUV and particle input, which can be constrained by the methods of Sections 3–5, would allow a direct test of whether a planet hosts the chemistry thought to have preceded life on Earth. Related "prebiosignature" programs have recently been proposed for the Habitable Worlds Observatory (HWO), which emphasize the need for near-ultraviolet coverage at 200–400 nm (Ranjan et al., 2025).

Several observational paths are opening. JWST transmission spectroscopy of rocky planets around nearby M dwarfs can already test for N_2O and NO_2 features in flare-processed atmospheres, although detecting them will require noise levels of a few ppm (Chen et al., 2021). The Extremely Large Telescope (ELT) will enable high-resolution reflected-light spectroscopy. A hybrid concept that pairs the ELT with a ∼100-m orbiting starshade, presented in my talk as HOEE (Hybrid Observatory for Earth-like Exoplanets), could deliver reflected-light spectra of Earth analogues around Sun-like stars over 300–1000 nm, including O_2 and H_2O features (Soliman et al., 2026). HWO will be the first mission designed to characterize ∼25 exo-Earths directly. A further, independent window is auroral emission. Energetic particles precipitating along a planet's magnetic field lines excite optical, UV and infrared auroral and airglow lines, such as the 557.7 nm oxygen line (Luger et al., 2017). Such emission would trace the same particle environment that drives pre-biosignature chemistry, and it would also reveal a planetary magnetic field.

9. Conclusions

Eighty years after Ambartsumian's discovery of stellar associations, Byurakan's legacy of studying young, active stars has become a foundation for identifying habitable planetary environments (Figure 10). The main points of this review are:

(1) Ambartsumian's 1947 insight that stars form continuously in young, expanding groups, and Byurakan's decades of work on T Tauri and flare stars, established that youth signifies magnetic activity. Young, active stars are the progenitors of the exoplanet hosts found by Kepler and TESS.

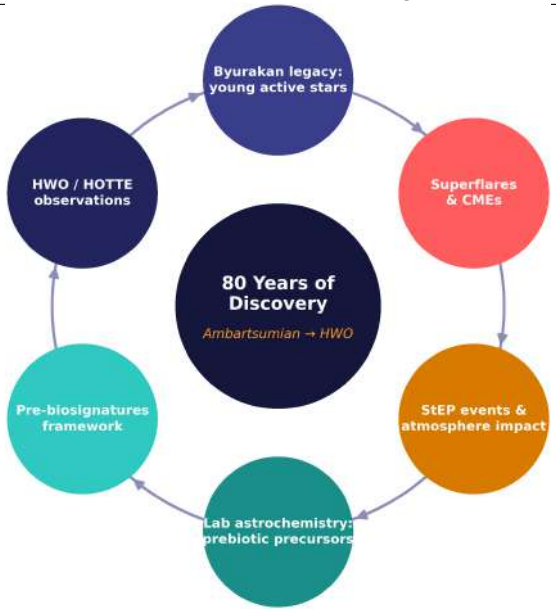

Figure 10. Eighty years of discovery, from Ambartsumian's young, active stars to the search for pre-biosignatures with the Habitable Worlds Observatory: young active stars → superflares and CMEs → StEP events and their atmospheric impact → laboratory astrochemistry of prebiotic precursors → the pre-biosignature framework → HWO and ground–space observations.

(2) Young solar analogues are saturated XUV emitters for ∼70 Myr, with EUV fluxes ∼100 times the present solar value. They produce superflares far more often than the present Sun, and PMS stars produce megaflares of up to $\sim 10^{38}$ erg. This activity obeys universal magnetic-flux scaling laws shared with the Sun.

(3) Superflares on young suns are accompanied by prominence eruptions and CMEs, now observed directly on EK Dra. Data-driven MHD and particle-acceleration models predict StEP fluences far above those of the largest modern SEP events. Corotating interaction regions in the winds of young suns, which a planet crosses every stellar rotation, drive magnetic storms of Carrington class on an Earth-like planet. They compress its magnetosphere to ∼2–3 R_E, open up to ∼60% of its magnetic flux and deposit up to ∼30 TW of Joule heating, which makes them as important as CMEs for atmospheric loss (Sur and Airapetian, 2025, Sur et al., 2026).

(4) StEPs are a double-edged sword. They contribute to atmospheric erosion, but they also drive deep-atmosphere chemistry that produces N_2O, HCN, formaldehyde, formamide and amino acids. Laboratory experiments show that proton irradiation is far more efficient than lightning or UV light in weakly reducing atmospheres.

(5) Particle-produced N_2O may help resolve the faint young Sun paradox. Together with HCN and other products, it defines a set of pre-biosignatures that JWST, the ELT, starshade hybrids and HWO can search for.

These results point to a natural extension of the program. The space weather of the parent star, together with the cosmic weather of Galactic cosmic rays modulated by the astrosphere as a star and its planets move through the Galaxy, does not stop at the top of a planetary atmosphere. It continues to shape the chemical and radiative environment at the surface over the whole history of a planet, so habitability is not a fixed property of an orbit but a concept that evolves with the star and its environment. Airapetian and Green (2026) proposed formalizing this connection as *heliobiology*, a new interdisciplinary field that links heliophysics, astrophysics, planetary science and chemistry with an astrobiological focus. They gave a formal definition of the field and a practical framework for its research agenda. Using the Sun–Earth system, where stellar input and biological response can both be measured, heliobiology offers a gateway to astrobiology: it provides the ground truth needed to interpret the space and cosmic weather of young stars, and the pre-biosignatures they drive, on exoplanets.

Ambartsumian taught us to see the Universe as young and evolving. Following his lead, the search for life is now being turned from a question of philosophy into one of physics, chemistry, laboratory experiments and observation.

Acknowledgements

I thank the organizers of the BAO 80th anniversary conference for the invitation. This review draws on work with many colleagues, including M. Jin, D. Sur, J. Hu, G. Gronoff, K. Kobayashi, K. Namekata, S. Toriumi, K. France, K. V. Getman, E. D. Feigelson, T. Sextro, K. Ikuta, Y. Notsu, K. V, G. Li, M. J. Way, A. Glocer, H. Maehara and K. Shibata, whose contributions I gratefully acknowledge. Vladimir S. Airapetian acknowledges support from the NASA/GSFC Internal Research and Development funds (IRAD) and Sellers Exoplanet Environments Collaboration (SEEC), the Fundamental Laboratory Research (FLaRe), which are funded by the NASA Heliophysics and Planetary Science Division's Internal Scientist Funding Model (ISFM) and NASA's Astrophysics Theory Program grant #80NSSC24K0776.

References

V. S. Airapetian and J. L. Green. *Nature Astronomy*, 10:1244, 2026.

V. S. Airapetian, A. Glocer, G. Gronoff, E. Hébrard, and W. Danchi. *Nature Geoscience*, 9:452, 2016.

V. S. Airapetian, A. Glocer, G. V. Khazanov, et al. *ApJL*, 836:L3, 2017.

V. S. Airapetian, R. Barnes, O. Cohen, et al. *International Journal of Astrobiology*, 19:136, 2020.

V. S. Airapetian, M. Jin, T. Lüftinger, et al. *ApJ*, 2021. doi: https://doi.org/10.3847/1538-4357/ac081e.

V. S. Airapetian, N. M. Curran, M. Jin, et al. *PNAS*, 2026. submitted.

R. L. Akeson, X. Chen, D. Ciardi, et al. *PASP*, 125:989, 2013.

V. A. Ambartsumian. *Stellar Evolution and Astrophysics*. Acad. Sci. Armenian SSR, Yerevan, 1947. in Russian.

V. A. Ambartsumian. *Astron. Zh.*, 26:3, 1949.

W. J. Borucki, D. Koch, G. Basri, et al. *Science*, 327:977, 2010.

S. Bryson, M. Kunimoto, R. K. Kopparapu, et al. *AJ*, 161:36, 2021.

H. Chen, Z. Zhan, A. Youngblood, et al. *Nature Astronomy*, 5:298, 2021.

L. I. Cleeves, E. A. Bergin, K. I. Öberg, et al. *ApJL*, 843:L3, 2017.

T. J. David, E. A. Petigura, R. Luger, et al. *ApJL*, 885:L12, 2019.

C. D. Dressing and D. Charbonneau. *ApJ*, 807:45, 2015.

E. D. Feigelson, G. P. Garmire, and S. H. Pravdo. *ApJ*, 572:335, 2002.

G. Feulner. *Reviews of Geophysics*, 50:RG2006, 2012.

K. France, G. Duvvuri, C. S. Froning, et al. *AJ*, 170:159, 2025.

K. V. Getman and E. D. Feigelson. *ApJ*, 916:32, 2021.

K. V. Getman, E. D. Feigelson, A. R. Waggoner, et al. *ApJ*, 976:195, 2024.

K. V. Getman, O. Kochukhov, J. P. Ninan, et al. *ApJ*, 980:57, 2025.

G. Gronoff, P. Arras, S. Baraka, et al. *JGR Space Physics*, 125:e2019JA027639, 2020.

M. Y. He, E. B. Ford, and D. Ragozzine. *AJ*, 161:16, 2021.

T. J. Henry, W.-C. Jao, J. P. Subasavage, et al. *AJ*, 132:2360, 2006.

A. W. Howard, G. W. Marcy, S. T. Bryson, et al. *ApJS*, 201:15, 2012.

J. Hu, V. S. Airapetian, G. Li, G. Zank, and M. Jin. *Science Advances*, 8:eabi9743, 2022.

K. Ikuta, K. Namekata, P. Petit, V. S. Airapetian, et al. *ApJ*, 2026. in press (arXiv:2602.15979).

A. H. Joy. *ApJ*, 102:168, 1945.

A. S. Kirichenko and S. A. Bogachev. *Solar Physics*, 292:120, 2017.

K. Kobayashi, J. Ise, R. Aoki, et al. *Life*, 13:1103, 2023.

K. Kobayashi, V. S. Airapetian, T. Udo, et al. *ApJL*, 1002:L12, 2026.

S. Koldobskiy, F. Mekhaldi, G. Kovaltsov, and I. Usoskin. *JGR Space Physics*, 128:e2022JA031186, 2023.

R. Luger, J. Lustig-Yaeger, D. P. Fleming, et al. *ApJ*, 837:63, 2017.

H. Maehara, T. Shibayama, S. Notsu, et al. *Nature*, 485:478, 2012.

F. Miyake, K. Nagaya, K. Masuda, and T. Nakamura. *Nature*, 486:240, 2012.

G. D. Mulders, I. Pascucci, and D. Apai. *ApJ*, 798:112, 2015.

K. Namekata, S. Toriumi, V. S. Airapetian, et al. *ApJ*, 945:147, 2023.

K. Namekata, V. S. Airapetian, P. Petit, et al. *ApJ*, 961:23, 2024.

K. Namekata, K. France, J. Chae, V. S. Airapetian, et al. *Nature Astronomy*, 10:64, 2025.

S. Okamoto, Y. Notsu, H. Maehara, et al. *ApJ*, 906:72, 2021.

B. H. Patel, C. Percivalle, D. J. Ritson, C. D. Duffy, and J. D. Sutherland. *Nature Chemistry*, 7:301, 2015.

E. A. Petigura, A. W. Howard, and G. W. Marcy. *PNAS*, 110:19273, 2013.

A. A. Pevtsov, G. H. Fisher, L. W. Acton, et al. *ApJ*, 598:1387, 2003.

P. Plavchan, T. Barclay, J. Gagné, et al. *Nature*, 582:497, 2020.

Ch. Rab, M. Güdel, M. Padovani, I. Kamp, W.-F. Thi, P. Woitke, and G. Aresu. *A&A*, 603:A96, 2017.

S. Ranjan, D. Adams, M. Wong, et al. arXiv:2507.00165, 2025.

C. Sagan and G. Mullen. *Science*, 177:52, 1972.

T. Sextro, V. S. Airapetian, et al. arXiv:2609.17683, 2026.

A. Soliman, J. Mather, S. Shaklan, et al. *Nature Astronomy*, 10:349, 2026.

D. Sur and V. S. Airapetian. *ApJ*, 994:75, 2025.

D. Sur, V. S. Airapetian, and M. Jin. *ApJL*, 2026. submitted.

S. Toriumi and V. S. Airapetian. *ApJ*, 927:179, 2022.

S. Toriumi, V. S. Airapetian, K. Namekata, and Y. Notsu. *ApJS*, 262:46, 2022.

V. Vasilyev, T. Reinhold, A. I. Shapiro, et al. *Science*, 386:1301, 2024.

M. J. Way, I. Aleinov, D. S. Amundsen, et al. *ApJS*, 231:12, 2017.

P. Woitke, I. Kamp, and W.-F. Thi. *A&A*, 501:383, 2009.

W. Zhu and S. Dong. *ARA&A*, 59:291, 2021.

W. Zhu, C. Petrovich, Y. Wu, S. Dong, and J. Xie. *ApJ*, 860:101, 2018.

J. Zhuleku, J. Warnecke, and H. Peter. *A&A*, 652:A32, 2021.

C. Zucker, A. A. Goodman, J. Alves, et al. *Nature*, 601:334, 2022.